Telescoping Jet Substructure

Yang-Ting Chien[a,d,*], Zachary Montague[a,b], Alex Emerman[c,d,e], Shih-Chieh Hsu[b], and Samuel Meehan[b]

[a] *Center for Theoretical Physics, Massachusetts Institute of Technology, Cambridge, MA 02139*
[b] *Department of Physics, University of Washington, Seattle, WA 98195*
[c] *Department of Physics, Columbia University, New York, NY 10027*
[d] *Theoretical Division, T-2, Los Alamos National Laboratory, Los Alamos, NM 87545*
[e] *Physics Department, Reed College, Portland, OR 97202*

(Dated: December 21, 2017)

We introduce a novel jet substructure method which exploits the variation of observables with respect to a sampling of phase-space boundaries quantified by the variability. We apply this technique to identify boosted W boson and top quark jets using telescoping subjets which utilizes information coming from subjet topology and that coming from subjet substructure. We find excellent performance of the variability, in particular its robustness against finite detector angular resolution. The extension to telescoping jet grooming and other telescoping jet substructure observables is also straightforward. This method provides a new direction in heavy particle tagging and suggests a systematic approach to the decomposition of jet substructure.

The Large Hadron Collider (LHC) has begun to probe physics above the electroweak scale, where the momenta of massive Standard Model particles are much larger than their invariant masses, resulting in hadronic decays of jets with prong-like substructures. Many jet substructure variables have been designed [1–3] and combined using multivariate techniques [4–7] to identify such jets and increase the sensitivity to beyond the Standard Model physics. The ability to reconstruct the jet features accurately is obscured by the presence of additional proton-proton interactions, i.e. pileup, as well as the underlying event of the hard collision, both of which cause additional radiation to fall within the catchment area of the jet. Often, this radiation is removed through a grooming procedure, e.g. [8–11]. Jet substructure observables and grooming procedures target certain intuitive features of the radiation properties and often have tuneable parameters. For example, the pruning parameters z_{cut} and D_{cut} control the softness and noncollinearity of a discarded particle. Conventionally, one makes a single choice of parameters deemed optimal by some metric. However, such a choice may neglect the full information the entire observable class contains.

Recently, Q-jets [12] introduced non-determinism in jet clustering. The procedure probes each jet multiple times and quantifies differences among pruned jets using the mass volatility. A similar goal is also achieved in [13]. Later, telescoping jets [14] probed the radiation pattern surrounding the dominant energy flow with multiple angular resolutions $\{R_i\}$ and extracted the full information contained in jets at all angular scales. In this Letter, we apply telescoping jets to analyze a set of commonly used jet observables and grooming procedures. We demonstrate the feasibility of this method as applied to the identification of hadronically decaying W bosons and top quarks, utilizing the variability of each observable induced by the variation of its parameters.

In hadronic boosted two-body resonance decays, such as that from a W boson, the resonance mass M introduces a two-prong structure in the jet at an angular scale $\Theta \approx 2M/p_T$ between the two prongs, where p_T is the transverse momentum of the heavy particle. On the other hand, QCD jets initiated by isolated quarks and gluons do not have such a distinct scale. However, when examining jets with masses near $M \pm \Delta m$, QCD jets are also two-prong-like but "fuzzier" when $\Delta m \gg \Gamma$, where Γ is the natural width of the resonance. Besides this nontrivial *subjet topology*, the strong interaction dictates the formation of subjets with *subjet substructures* and *subjet superstructures* [15] which are sensitive to the partonic origins of subjets.

In the case of boosted top quarks, the top mass (M_t) and the W mass (M_W) are similar. Therefore $\Theta_t \approx 2M_t/p_T^t$ and $\Theta_W \approx 2M_W/p_T^W$ are comparable. This results in the generic three-prong structure in the hadronic top decay $t \to W + b \to q_1 + q_2 + b$. However, when examining jets with a mass near $M_t \pm \Delta m$ the selected QCD jets are, again, two-prong-like, so observables which distinguish three-prong jets from two-prong jets will help discriminate QCD jets from true top quark jets.

Given an arbitrary jet observable $\mathcal{O}$ with a parameter a, the variation of the observable with respect to the sampling of parameters $\{a_i\}$ within $(a_{\min}, a_{\max})$ is quantified by the coefficient of variation $v_{\mathcal{O}}$ defined as the ratio of the standard deviation $\sigma(\mathcal{O})$ and the mean $\langle \mathcal{O} \rangle$ of $\{\mathcal{O}_{a_i}\}$,

$$v_{\mathcal{O}} = \frac{\sigma(\mathcal{O})}{\langle \mathcal{O} \rangle} \ . \qquad (1)$$

The $v_{\mathcal{O}}$ observable is referred to as the *variability*. Analogous to the first derivative in calculus, the variability $v_{\mathcal{O}}$ measures the change of the observable $\mathcal{O}$ with respect to the change of the phase-space boundary set by the parameter a. Instead of combining observables with different parameters in a multivariate analysis, the variability can give a trend of the observable variation which itself can be used as a distinguishing feature to classify jets.
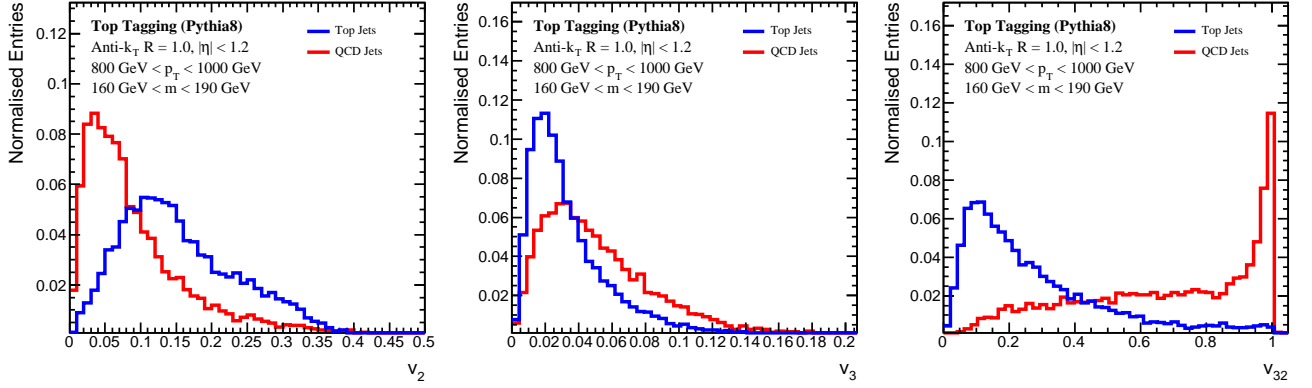
FIG. 1. The distributions of the variabilities v_2 (left panel) and v_3 (middle panel), as well as their ratio v_{32} (right panel) for top and QCD jets with 800 GeV $< p_T <$ 1 TeV and 160 GeV $< m <$ 190 GeV using the truth-particle information.

We focus on the variability of the jet mass with respect to varying the parameters which determine the jet constituents contributing to the jet mass. The sampling of the telescoping parameters is chosen to be uniform within the range $(a_{\min}, a_{\max})$. We outline the procedure of *telescoping subjets*: N subjets are reconstructed exclusively around dominant energy flows within a jet. A similar method using the leading subjets in a reclustered jet was explored in [16]. We groom the jets using the trimming algorithm with $R_{\mathrm{sub}} = 0.3$ and $f_{\mathrm{cut}} = 0.05$ to remove underlying event contaminations. Although we do not include pileup in our studies, using groomed jet constituents can also mitigate the pileup effect. We choose the subjet axes as the N-subjettiness axes [17] with $\beta = 1$ and build subjets around them with radius R_T within the voronoi regions [18–21]. Particles are assigned to the nearest axis according to the distance ΔR_{ij} between the axis $\hat{n}_i$ and particle p_j,

$$\mathrm{subjet}_i = \{p_j \mid \Delta R_{ij} < R_T \text{ and } \Delta R_{ij} < \Delta R_{kj} \ , \ \forall k \neq i\}, \tag{2}$$

where k is the index of the other axes $\hat{n}_k$. The variability v_N (the shorthand notation of v_{m_N}) of the invariant masses of the sum of N subjets is reconstructed with the telescoping parameter $a = R_T \in (0.1, 1.0) \times R$. Note that $a_{\max}$ is chosen to be the jet radius R to scan through the entire catchment area of the jet. On the other extreme, the dominant energy features will be lost if a is too small, so $a_{\min}$ is chosen as $0.1 \times R$. We focus on $N = 2$ and 3 in W and $N = 2$, 3, and 4 in top tagging, but N could be extended further for more exotic boosted topologies.

The generality of the telescoping algorithm allows a variety of other telescoping applications which are, however, beyond the scope of this Letter. For example, in *telescoping pruning* one can fix z_{cut} and construct v_{prun}, the variability of the pruned jet mass with the telescoping parameter a in $D_{\mathrm{cut}} = a \ 2m_{\mathrm{jet}}/p_{T_{\mathrm{jet}}}$. In *telescoping trimming*, one can fix the subjet radius R_{sub} and construct v_{trim}, the variability of the trimmed jet

mass with the telescoping parameter $a = f_{\mathrm{cut}}$. One can also construct v_{τ_N}, the variability of the N-subjettiness with the telescoping parameter $a = \beta$ [22]. Correlations among variations with respect to multiple varied parameters can also be explored.

Besides variabilities, useful angular observables, which encode information about subjet topology, and mass observables, which reveal the presence of specific decay products, can be obtained seamlessly from the telescoping subjet algorithm. For instance, in W tagging with $N = 2$, the subjet topology is affected by the jet mass cut, but W and QCD jets can still have significantly different distributions for the angle θ_2 between the two dominant energy flows. For top tagging with $N = 3$, we consider the minimal angle $\theta_{\min}$ among the subjet axes. For QCD jets typically with two prongs, two of the three axes tend to be close to each other; therefore, $\theta_{\min}$ is expected to be small. For top jets with three prongs, this angle is distributed away from zero. Also, we attempt to identify the W inside the top jet [23, 24] by considering m_{W2}, the invariant mass of two of the three exclusive voronoi regions closest to the W mass, and the variability $v_{m_{W2}}$ of the di-subjet invariant masses within those two regions.

The study is performed using samples generated from Monte Carlo simulations of proton-proton collisions at $\sqrt{s} = 13$ TeV using PYTHIA8 [25]. Particles are clustered into jets with FASTJET 3 [26] using the anti-k_T algorithm [27] with $R = 1.0$ and are required to be central with a pseudorapidity $|\eta| < 1.2$. We consider two kinematic regimes where the jet p_T is either between 350 GeV and 500 GeV or 800 GeV and 1 TeV. Signal W boson and top quark jets are generated using decays of heavy Kaluza-Klein gravitons with invariant masses at 1 or 2 TeV for the two p_T bins in fully hadronic $G^* \rightarrow W^+W^-$ and $G^* \rightarrow t\bar{t}$ processes. Background QCD jets are generated from the Standard Model dijet process. To study the impact of finite detector resolution, we compare the results with the particles clustered in
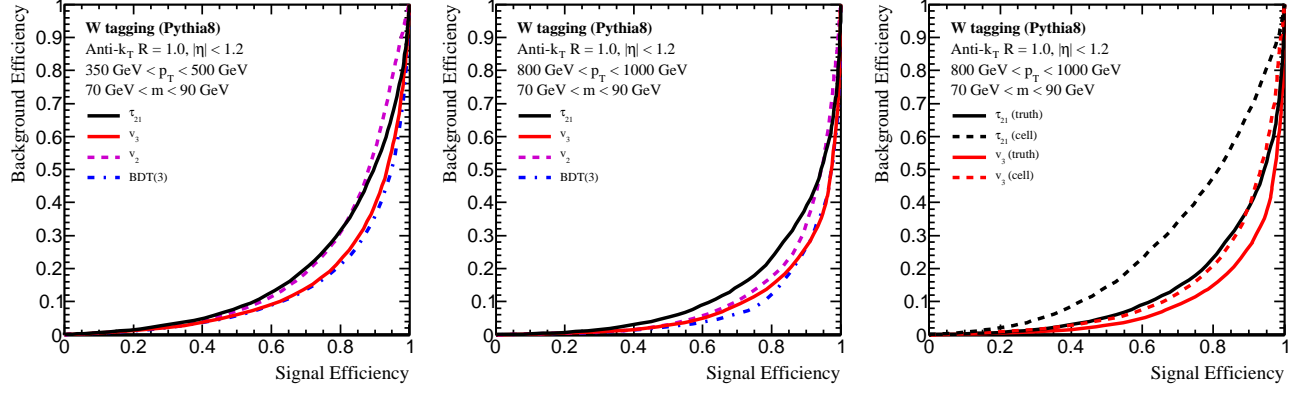
FIG. 2. The W tagging ROC curves of the variabilities v_2 and v_3; the BDT combinations of three telescoping subjets variables $\{v_2, v_3, \theta_2\}$; and the two-prong tagger $\tau_{21} = \tau_2/\tau_1$ in the $(300 \text{ GeV}, 500 \text{ GeV})$ jet p_T bin (left panel) and the $(800 \text{ GeV}, 1 \text{ TeV})$ bin (middle panel). Right panel: ROC curves of v_3 and τ_{21} in the $(800 \text{ GeV}, 1 \text{ TeV})$ jet p_T bin. Solid curves correspond to the ones with the truth-particle information, and the dashed curves are the ones using the pseudo-calorimeter cell particle information.

pseudo-calorimeter (η, ϕ) cells of size 0.1×0.1, with each cell momentum constructed with zero mass and direction from the primary vertex. A selection on the trimmed jet mass is made between 70 GeV and 90 GeV for W tagging and between 160 GeV and 190 GeV for top tagging.

To examine the complementarity of the information contained in the telescoping subjet variables, subsets of them are inputs for Boosted Decision Trees (BDTs) implemented in TMVA [28]. For top tagging we also consider the ratio v_{N2} between v_N and v_2 for $N = 3, 4$,

$$v_{N2} = \frac{v_N}{v_2} \ . \tag{3}$$

Shown in Figure 1 are the distributions of v_2, v_3, and v_{32} for top and QCD jets. We find that top jets have a broader v_2 distribution and a narrower v_3 distribution. The large variation of the jet mass when telescoping around the two subjet axes is caused by the transition of the W from being partially reconstructed to fully reconstructed. There is not an intrinsic mass scale dictating the third hard emission for QCD jets. On the other hand, the three prongs inside top jets are quark-initiated subjets, whereas the subjets in QCD jets can have gluonic origins. Quark subjets are narrower than gluon subjets; therefore v_3 of top jets tend to be smaller. The v_{32} observable has almost the same performance as the BDT with input $\{v_2, v_3\}$, suggesting that v_{32} may be the optimal way of combining the two variabilities.

An interesting feature of v_{32} is that it cuts off naturally at 1, most clearly seen in QCD jets. Crucially, $v_3 \leq v_2$ in the collinear limit. The two-prong structure in QCD jets implies that v_2 and v_3 collect similar information. The third energy flow axis can not be displaced far from the two axes determined at $N = 2$. Hence, little new information is collected by constructing a third subjet and the distribution of v_{32} for QCD jets peaks at 1. In

the case where there is a third, semi-hard emission, the emission is captured by all telescoping subjets at $N = 3$ and does not induce the observable variation and so $v_3 < v_2$. In general, for larger N, more particles are captured by-default and so the variability is expected to decrease $(v_{N+1} \leq v_N)$.

The background efficiency as a function of the signal efficiency is illustrated by receiver operating characteristic (ROC) curves, where a lower curve indicates a better tagging performance. Shown in Figure 2 are the ROC curves of v_2, v_3, the BDT combinations of the telescoping subjet variables $\{v_2, v_3, \theta_2\}$, and the two-prong tagger $\tau_{21} = \tau_2/\tau_1$ in W tagging. The left and middle panels correspond respectively to two jet p_T regions of $(350 \text{ GeV}, 500 \text{ GeV})$ and $(800 \text{ GeV}, 1 \text{ TeV})$. Overall, the tagging performance increases at higher p_T, demonstrating the general advantage of applying telescoping jets to the boosted regime. In the right panel, we compare the tagging performance using truth particles and pseudo-calorimeter clusters, which degrade information about structures smaller than the cell size. We find excellent performance of v_3. Also, the v_3 observable is much more robust against pseudo-calorimeter smearing, especially at high p_T, showing its qualitatively different feature compared to τ_{21}. The telescoping procedure in the v_3 observable utilizes the rapid depletion of radiation around the W at larger angles in the boosted regime. This "W isolation" effect is the manifestation of the fact that the W is a color singlet which affects the color structure of the subjets and the radiation pattern at large angles. The time dilation that occurs before W hadronically decays can also result in a period of time, about $\mathcal{O}(1) \text{ fm}/c$ [29], in which no QCD radiation is emitted. There is no such gap in the jet formation process for QCD jets. On the other hand, the fact that v_3 performs better than v_2 hints at the significance of a third, semi-hard emission in W
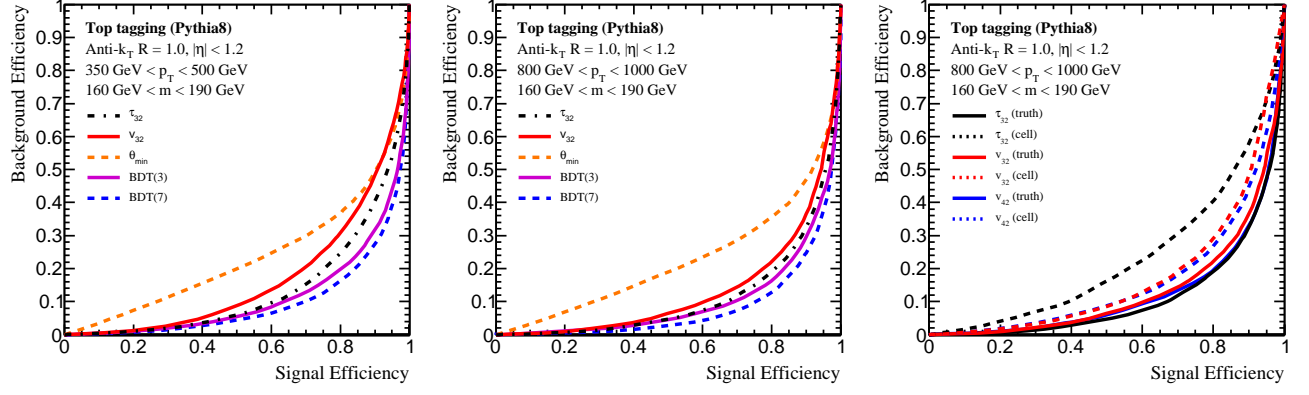
FIG. 3. The top tagging ROC curves of the variability ratio v_{32}, the minimal angle among three subjets $\theta_{\min}$, the BDT combinations of three and seven telescoping subjets variables $\{m_{W2}, v_2, v_3\}$ and $\{\theta_2, \theta_{\min}, m_{W2}, v_2, v_3, v_4, v_{m_{W2}}\}$, and the three-prong tagger $\tau_{32} = \tau_3/\tau_2$ in the $(300 \text{ GeV}, 500 \text{ GeV})$ jet p_T bin (left panel) and the $(800 \text{ GeV}, 1 \text{ TeV})$ bin (middle panel). Right panel: ROC curves of v_{32}, v_{42} and τ_{32} in the $(800 \text{ GeV}, 1 \text{ TeV})$ jet p_T bin. Solid curves correspond to the ones with the truth-particle information, and the dashed curves are the ones using the pseudo-calorimeter cell particle information.

and QCD jets. The v_3 observable disentangles such an emission when quantifying the isolation of W jets.

Shown in Figure 3 are the ROC curves for top tagging performance including v_{N2} ($N = 3, 4$), $\theta_{\min}$, the BDT combinations of telescoping subjets variables $\{v_2, v_3, m_{W2}\}$ and $\{\theta_2, \theta_{\min}, m_{W2}, v_2, v_3, v_4, v_{m_{W2}}\}$, and the three-prong tagger $\tau_{32} = \tau_3/\tau_2$. Again, the left and middle panels correspond to the two kinematic regimes $p_T \in (350 \text{ GeV}, 500 \text{ GeV})$ and $p_T \in (800 \text{ GeV}, 1 \text{ TeV})$, and we note tagging performance increases at higher p_T. In the right panel, the ROC curves plot both truth-particle and pseudo-calorimeter information. We find the excellent performance of v_{N2} and its robustness against pseudo-calorimeter smearing, especially at high p_T where the performance of the more conventionally used τ_{32} observable degrades dramatically. This indicates the qualitatively different features of v_{N2} and a three-prong tagger. We also find the usefulness of including m_{W2} in the minimal BDT combination which significantly increases the tagging performance. It is clear that the intrinsic mass scale M_W within the top jet is a unique feature distinguishing itself from the QCD background. Similar to the fact that v_3 performs better than v_2 in W tagging, the v_{42} observable has a better performance than v_{32}, suggesting the significance of a fourth, semi-hard emission in top jets. One starts to see the W isolation within the top jet in the boosted regime.

To conclude, we introduce a qualitatively new jet substructure method using variability to quantify the change of observables with respect to a sampling of the phase-space boundaries in the observable definition. This technique is general and can be used to analyze arbitrary classes of jet substructure observables and grooming procedures. In W and top tagging, we find excellent performance of telescoping subjets quantified by v_3 in W tagging and v_{42} in top tagging. Furthermore, their robustness is found to be significantly better than more widely used N-prong taggers such as N-subjetiness via a comparison of the performance between reconstruction from using truth particles and from a pseudo-calorimeter.

The new physics messages we learn include the emergence of the isolation of W jets at high p_T, which is a dominant feature over their two-prong structure. This is true for all other heavy, color-singlet Standard Model particles including the Z and the Higgs boson. It would be promising to include this feature in their tagging strategies. The top jet also has features beyond the three-prong structure which can be exploited to increase tagging performance. The telescoping subjets provides a systematic framework within which one can construct qualitatively new jet substructure observables. This paves the road toward systematic jet studies using telescoping deconstruction [30].

———————

* ytchien@mit.edu

[1] A. Abdesselam *et al.*, *Boost 2010 Oxford, United Kingdom, June 22-25, 2010*, Eur. Phys. J. **C71**, 1661 (2011), arXiv:1012.5412 [hep-ph].

[2] A. Altheimer *et al.*, *BOOST 2011 Princeton , NJ, USA, 22V26 May 2011*, J. Phys. **G39**, 063001 (2012), arXiv:1201.0008 [hep-ph].

[3] A. Altheimer *et al.*, *BOOST 2012 Valencia, Spain, July 23-27, 2012*, Eur. Phys. J. **C74**, 2792 (2014), arXiv:1311.2708 [hep-ex].

[4] D. Adams *et al.*, Eur. Phys. J. **C75**, 409 (2015), arXiv:1504.00679 [hep-ph].

[5] A. J. Larkoski, I. Moult, and B. Nachman, (2017), arXiv:1709.04464 [hep-ph].

[6] ATLAS Collaboration, ATLAS-CONF-2017-064, (2017).

[7] CMS Collaboration, JHEP **12**, 017. 43 p (2014),.

[8] S. D. Ellis, C. K. Vermilion, and J. R. Walsh, Phys.Rev. **D80**, 051501 (2009), arXiv:0903.5081 [hep-ph].

[9] D. Krohn, J. Thaler, and L.-T. Wang, JHEP **1002**, 084 (2010), arXiv:0912.1342 [hep-ph].

[10] M. Dasgupta, A. Fregoso, S. Marzani, and G. P. Salam, JHEP **09**, 029 (2013), arXiv:1307.0007 [hep-ph].

[11] A. J. Larkoski, S. Marzani, G. Soyez, and J. Thaler, JHEP **05**, 146 (2014), arXiv:1402.2657 [hep-ph].

[12] S. D. Ellis, A. Hornig, T. S. Roy, D. Krohn, and M. D. Schwartz, Phys. Rev. Lett. **108**, 182003 (2012), arXiv:1201.1914 [hep-ph].

[13] L. Mackey, B. Nachman, A. Schwartzman, and C. Stansbury, JHEP **06**, 010 (2016), arXiv:1509.02216 [hep-ph].

[14] Y.-T. Chien, D. Farhi, D. Krohn, A. Marantan, D. Lopez Mateos, and M. Schwartz, JHEP **12**, 140 (2014), arXiv:1407.2892 [hep-ph].

[15] J. Gallicchio and M. D. Schwartz, Phys. Rev. Lett. **105**, 022001 (2010), arXiv:1001.5027 [hep-ph].

[16] Y. Cui, Z. Han, and M. D. Schwartz, Phys.Rev. **D83**, 074023 (2011), arXiv:1012.2077 [hep-ph].

[17] J. Thaler and K. Van Tilburg, JHEP **02**, 093 (2012), arXiv:1108.2701 [hep-ph].

[18] I. W. Stewart, F. J. Tackmann, and W. J. Waalewijn, Phys. Rev. Lett. **105**, 092002 (2010), arXiv:1004.2489 [hep-ph].

[19] Y.-T. Chien, Phys. Rev. **D90**, 054008 (2014), arXiv:1304.5240 [hep-ph].

[20] I. W. Stewart, F. J. Tackmann, J. Thaler, C. K. Vermilion, and T. F. Wilkason, JHEP **11**, 072 (2015), arXiv:1508.01516 [hep-ph].

[21] J. Thaler and T. F. Wilkason, JHEP **12**, 051 (2015), arXiv:1508.01518 [hep-ph].

[22] J. Thaler and K. Van Tilburg, JHEP **03**, 015 (2011), arXiv:1011.2268 [hep-ph].

[23] J. Thaler and L.-T. Wang, JHEP **07**, 092 (2008), arXiv:0806.0023 [hep-ph].

[24] D. E. Kaplan, K. Rehermann, M. D. Schwartz, and B. Tweedie, Phys. Rev. Lett. **101**, 142001 (2008), arXiv:0806.0848 [hep-ph].

[25] T. Sjostrand, S. Mrenna, and P. Z. Skands, Comput. Phys. Commun. **178**, 852 (2008), arXiv:0710.3820 [hep-ph].

[26] M. Cacciari, G. P. Salam, and G. Soyez, Eur. Phys. J. **C72**, 1896 (2012), arXiv:1111.6097 [hep-ph].

[27] M. Cacciari, G. P. Salam, and G. Soyez, JHEP **0804**, 063 (2008), arXiv:0802.1189 [hep-ph].

[28] A. Hoecker, P. Speckmayer, J. Stelzer, J. Therhaag, E. von Toerne, and H. Voss, PoS **ACAT**, 040 (2007), arXiv:physics/0703039.

[29] L. Apolinario, J. G. Milhano, G. P. Salam, and C. A. Salgado, (2017), arXiv:1711.03105 [hep-ph].

[30] Y.-T. Chien and R. K. Elayavalli, to appear soon (2017).